Available on CMS information server **CMS NOTE 1997/075**

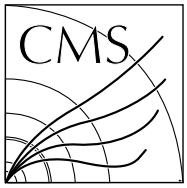


**The Compact Muon Solenoid Experiment**

# CMS Note

Mailing address: CMS CERN, CH-1211 GENEVA 23, Switzerland

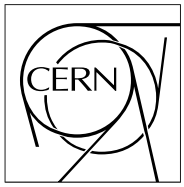


**August 1997**

# Prototype analogue optical links for the CMS tracker readout system

V. Arbet-Engels, G. Cervelli, K. Gill, R. Grabit, C. Mommaert, G. Stefanini, and F. Vasey
*CERN, CH-1211, Geneva 23, Switzerland.*

**Abstract**

The optical fibre links for the analogue readout of the CMS tracker are based on the direct modulation of edge-emitting lasers located inside the detector volume. The front-end signals are transmitted by single-mode optical fibres and detected in the counting room using PIN photodiodes. One channel link demonstrators consisting of commercially available optoelectronic devices have been fully characterized. The lasers, fibres, and PIN diodes are representative of the devices intended to be used in the final system. The link overall performance is discussed in terms of its static and dynamic responses and is shown to meet the technical specifications of the full readout chain.

# 1 Introduction

Data signals from the $12x10^6$ microstrip detector channels of the CMS tracker will be transferred to the counting room via over 50,000 analogue fibre optic links [1]. Following a R&D program of over several years during which different optical data transmission technologies have been investigated [2-4], it was concluded that the best combination fulfilling the optical link requirements and development timescales is based on directly modulated edge-emitting laser transmitters, single mode optical fibres, and PIN photodiode receivers.

In the present note, we report on the technical performance of a one-channel link demonstrator. Characteristics of both transmitter and receiver as well as the full link transfer function are presented. The functionality of the analogue optical link within the readout system along with its requirements are first briefly reviewed.

# 2 Link functionality

## 2.1 Overview of the system

The silicon and gas microstrip detectors are read out by charge sensitive amplifiers whose voltages are sampled at the beam crossing rate of 40 MHz. During the level-1 trigger latency, the samples are stored in the analogue memories of the front-end APV chips [5] for up to 3.2 μs. Following a trigger, each of the 50,000 fibre links transmits signals from 256 detector channels at a rate of 40Msamples/s to the digitizers of the front-end driver modules (FED) in the counting room. A more detailed description of the readout chain can be found elsewhere [6].

## 2.2 Technical constraints

In order to achieve sufficient resolution to transfer signals equivalent to several MIPs, the performance required from the link can be summarized as follows: (a) full scale dynamic range of 7-8 bits, with < 2% deviation from linearity, (b) overall link noise contribution (rms) equivalent to less than one third of the least significant bit (LSB), and (c) settling time of 15ns to within 1% of the end value. These figures are not very demanding for today's optoelectronic technologies. However, they must be achieved and maintained in the challenging front-end environment and at a low cost. All the optoelectronic components situated at the front-end will be subjected to high radiation levels. Over the projected 10 years of operation, the integrated dose and hadronic fluences in the tracker volume are estimated to be of the order of 10Mrad (100KGy) and a few $10^{14}$ (neutron equivalent)/$cm^2$

(<E>=1MeV), respectively [7-9]. The effects of gamma and neutron irradiations on laser diodes, PIN diodes, and fibres are the subject of ongoing studies [10-12]. The results obtained so far indicate very good radiation hardness. Other technical constraints on the front-end components include low power dissipation, low mass, operation in a magnetic field of up to 4T, and very limited accessibility for maintenance services [13].

## 3 Link description

A simplified representation of the analogue fibre link connecting the tracker front-end to the readout electronics is sketched in Fig. 1. The link is unidirectional, about 100m long, and uses directly modulated edge emitting lasers. The laser diode converts electrical detector signals into optical signals, which are then transmitted by a single mode fibre to the FED board and finally received by a PIN photodiode [14].

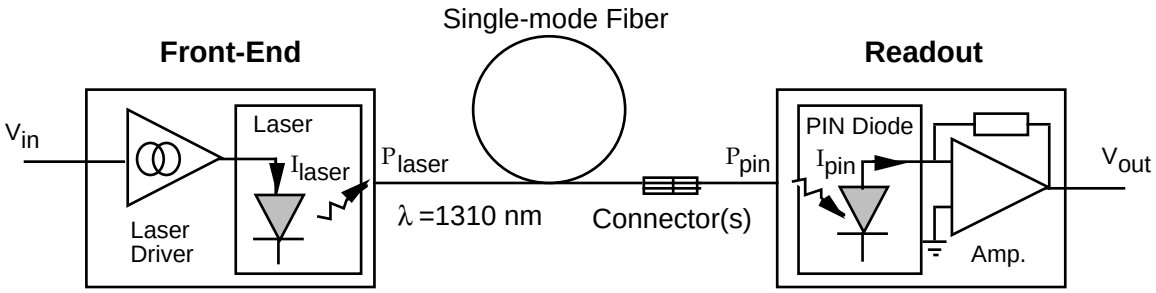


Fig. 1 : Schematic of the analogue link with the transmitter (left) and the receiver (right) modules.

A one channel link prototype with the above configuration has been successfully built and tested. The optoelectronic devices are commercially available products supplied by Italtel (Milano) and are of the same type as the ones intended for the final system. The laser driver and photodiode amplifier are custom developments built from off- the-shelf discrete IC's mounted onto small printed circuit boards. A driver ASIC in full rad-hard technology has been designed and is being presently evaluated.

In the following, the analogue transmitter and receiver are described. It is worth noting that to fully characterize the electrical to optical (E/O) transmitter module, a reference high bandwidth optical detector is required. The same applies to the receiver module with a calibrated optical source. Without these devices (with known technical specifications), the measurement procedure suffers from lack of accuracy. By staying in the electrical domain

during the full link evaluation, this experimental difficulty is avoided. The full link results are presented in paragraph 4.

### 3.1 Analogue transmitter

The analogue transmitter is illustrated in Fig. 2. It includes the semiconductor laser and the laser driver.

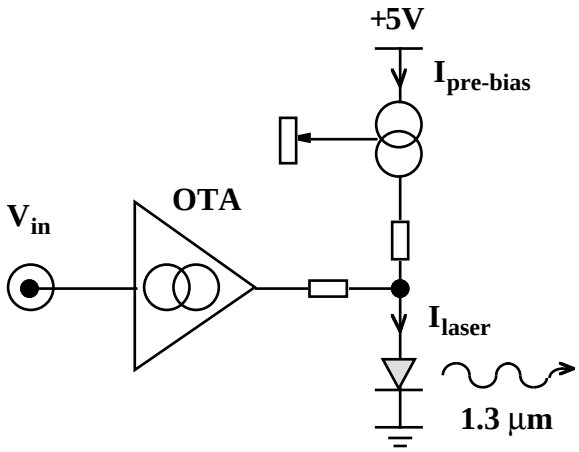


Fig. 2 : Analogue transmitter with the transconductance amplifier (OTA) and the pre-biasing circuitry.

#### 3.1.1 Laser diode

The laser structure is of the double-channel planar buried heterostructure (DCPBH) type with an InGaAsP strained multiple quantum well active region grown on top of an InP substrate [15]. Cleaved facets define the optical Fabry-Perot cavity. The laser emission wavelength occurs at 1.3μm from band to band transitions in the strained quantum wells. A typical laser transmitter L-I curve is shown in Fig. 3. The two important extracted parameters are the threshold current, $I_{th}$, and the slope efficiency, $\eta$ ($\eta = dP_{laser} / dI_{laser}$). The threshold current sets the limit above which stimulated emission builds up at the expense of the non-coherent spontaneous emission and optical gain balances the total losses. The slope efficiency specifies the amount of output light power coupled into the fiber per injected drive current above threshold. The investigated lasers have a typical threshold current close to 8 mA and a slope efficiency $\eta \approx 0.22$ W/A. The laser die and fibre are actively aligned to each other and mounted onto a common Si-submount with footprint dimensions ≈ 2x1.5 mm, as illustrated in Fig. 4. The resulting compact and low mass sub-assembly is further hermetically encapsulated into a mini-DIL (dual-in-line) ceramic package.

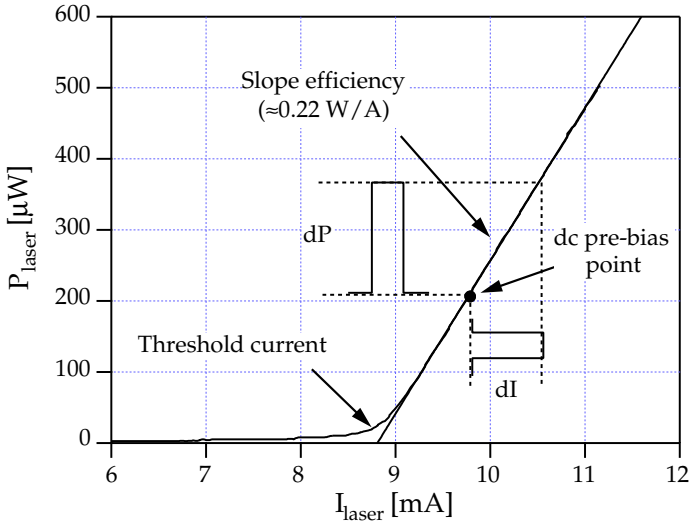


Fig. 3 : Typical L-I curve of the semiconductor laser transmitter indicating the threshold current, dc pre-bias point, and slope efficiency.

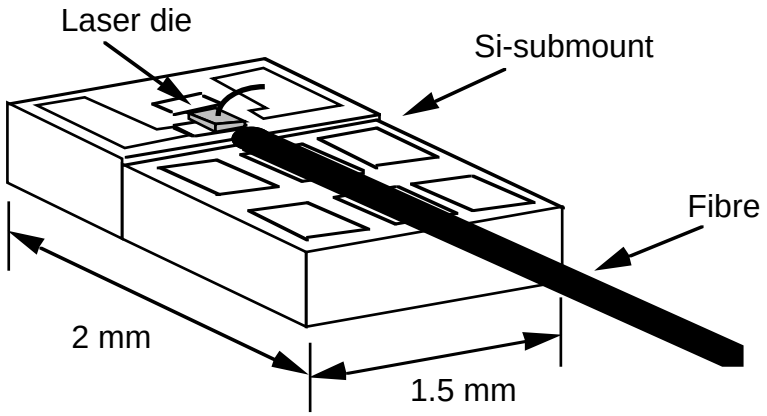


Fig. 4 : Laser assembly showing the Si-submount, laser, and optical fibre.

### 3.1.2 Laser driver

*Static characteristic*

The laser driver provides the dc pre-bias current, $I_{pre\text{-}bias}$, as well as the modulation current proportional to the input voltage signal $V_{in}$ (Fig. 2). The pre-bias working point is set by adjusting the reference input resistor of a monolithic dual transistor current mirror. The modulation current is controlled by a wide bandwidth (370MHz) operational transconductance amplifier (OTA). The static characteristic of the laser driver is shown in Fig. 5 (a) for three different pre-bias conditions : 4 mA, 10 mA, and 20 mA, respectively.

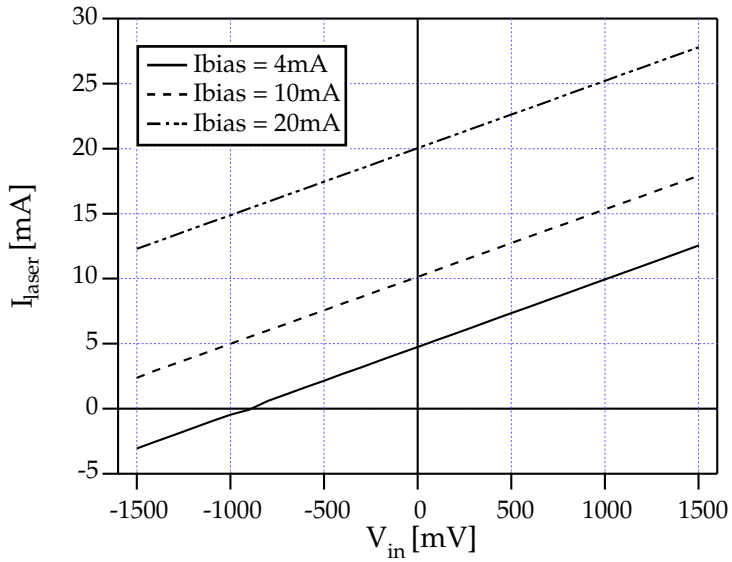


(a)

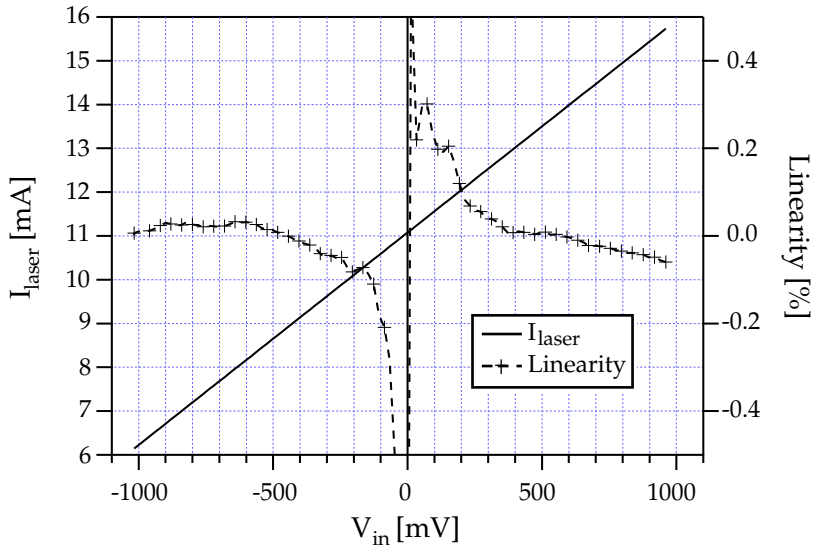


(b)

Fig 5: (a) Static characteristic of the laser driver for three different pre-bias current values. (b) Linearity for the case of $I_{pre\text{-}bias}$ = 11 mA.

The total laser current, $I_{laser}$, corresponds to the sum of the constant dc pre-bias current and the adjustable modulation current. The measured transconductance, $G_m$, is 5.2 mA/V and is independent of the pre-bias point. Hence, multiplying $G_m$ by the laser slope efficiency $\eta$, the transmitter gain is calculated to be 1.14 $\mu$W/mV.

The analogue driver relative deviation from linearity (RDL) for a dc pre-bias current of 11 mA is shown in Fig. 5 (b). It is defined as the relative distortion with respect to a linear fit and is expressed as follows:

$$\text{RDL [\%]} = 100 \times \frac{I_{\text{laser-exp.}} - I_{\text{laser-fit}}}{I_{\text{laser-fit}} - I_{\text{pre-bias}}} \quad (1)$$

where $I_{\text{laser-exp.}}$ is the experimental current value, $I_{\text{laser-fit}}$ a best linear fit for input signals in the range of ± 900 mV, and $I_{\text{pre-bias}}$ the dc pre-bias current or 11 mA in the present case. The linearity remains well below one percent with diverging values for $V_{\text{in}}$ close to 0 mV since at the origin, $(I_{\text{laser-fit}} - I_{\text{pre-bias}}) \approx 0$ and the function becomes undefined.

*Dynamic characteristic*

In order to evaluate the dynamic characteristics of the driver alone, the laser cannot simply by replaced by a resistor since a resistor is not representative of the actual laser impedance at high frequencies. Work is currently in progress to measure the intrinsic bandwidth of the complete transmitter using a wide bandwidth O/E converter.

The time delay of the transmitter board was estimated by sending a pulsed input signal and by looking at the delay between the input and output on an oscilloscope for varying input coax cable lengths. Extrapolating to "0" cable length, an overall time delay of ≈ 1.8ns was deduced for the present driver configuration.

### 3.2 Analogue receiver

A schematic of the analogue receiver module is shown in Fig. 6. It includes the PIN photodiode and the amplifier.

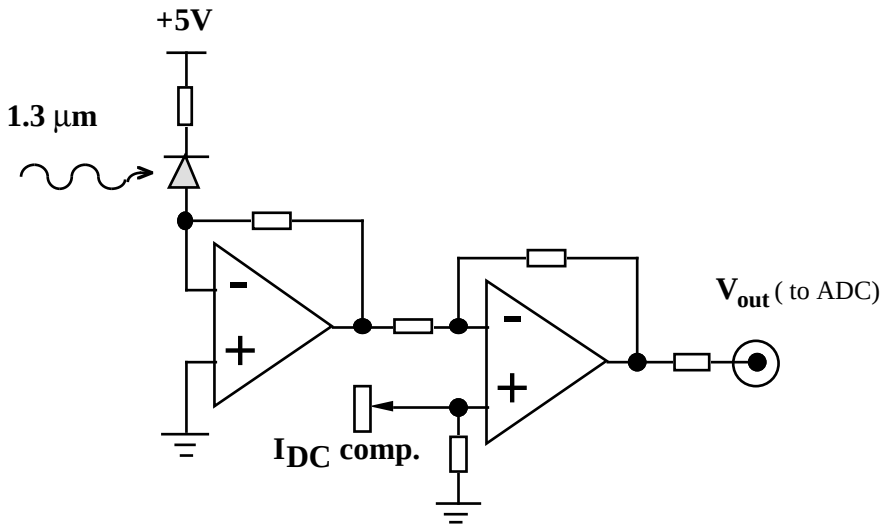


Fig. 6 : Analogue receiver showing the reverse biased PIN photodiode and the transimpedance amplifier.

### 3.2.1 Photodiode

The PIN photodiodes consist of a lattice matched InGaAs alloy active layer grown on top of an InP substrate [16]. A heavily doped p-type implant defines the active diameter of ≈ 75 μm. The intrinsic i-region serves to enhance the light collection efficiency by extending the width of the depletion layer in addition to reducing the junction capacitance [17]. Impinging photons at 1.3μm generate electron-hole pairs in InGaAs that quickly drift in opposite directions under the influence of the strong electric field in the depletion region. As a result, a photocurrent proportional to the light intensity is produced in the external circuit. The factor of proportionality corresponds the photodiode responsivity, $R_{pin}$, and is ≈ 0.96 A/W (at 1.3μm) for the tested diodes. A typical photodiode response curve is shown in Fig. 7 for optical power up to 1 mW.

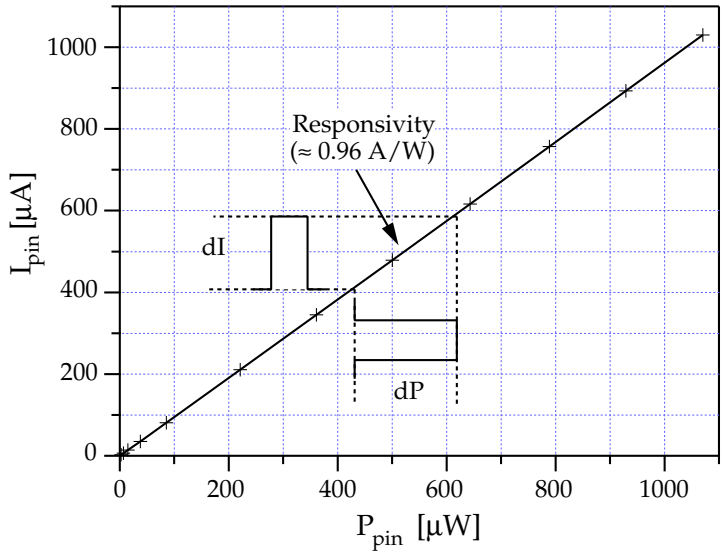


Fig. 7: Photocurrent vs. light power for a representative PIN photodiode.

The PIN photodiodes are back illuminated with the InP substrate acting as a transparent optical window at 1.3 μm. The fibre light is coupled to the photodiode chip through the use of an angle etched Si-submount onto which both the fibre and the photodiode are attached. The packaging scheme is similar to the laser module with a small footprint Si-submount housed in a mini-DIL package. The silicon sub-assembly (OSA) with the fibre-pigtailed PIN photodiode is illustrated in Fig. 8.

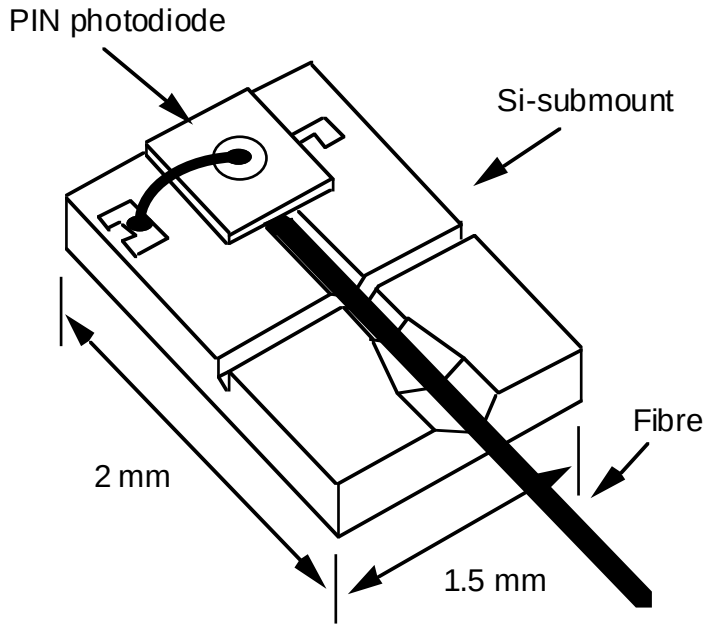


Fig. 8: Photodiode assembly showing the Si-submount, photodiode, and optical fibre.

### 3.2.2 Photodiode amplifier

*Static characteristic*

The photocurrent of the reverse biased PIN photodiode is converted to a voltage using a transimpedance amplifier (Fig. 6) [18]. In the final readout system, the voltage output of the amplifier will be connected to the input of the ADC converter on the FED board. The photodiode is dc-coupled to the amplifier thus allowing the on-line monitoring of the quasi-static link performance. A compensation network adapts the receiver operating range to the transmitter dc pre-bias point. The static response of the amplifier is illustrated in Fig. 9 for an offset bias of 0V. The photocurrent, $I_{pin}$, was simulated by injecting a signal into a 10kΩ resistor. The measured transresistance gain, $R_{Rx} \approx 9.93$ kΩ, translates to a receiver gain of 9.53 mV/μW if multiplied by the photodiode responsivity ($R_{pin} = 0.96$A/W). The amplifier saturates at ±3.2V for an input current range of ±350 μA. To this 700 μA current signal would correspond an injected optical power range (above the laser dc pre-bias point) of ≈ 730 μW. Obviously, such large optical power ranges are only achieved by properly adjusting the offset of the compensation network (since the photodiode can only supply positive photocurrents entering the input stage of the amplifier).

The RDL is plotted on the right axis of Fig. 9, representing the relative error from a linear fit over a photocurrent range of ±300 μA. It is less than 0.2% and it is calculated using the same method as for the laser driver RDL (Eq. 1).

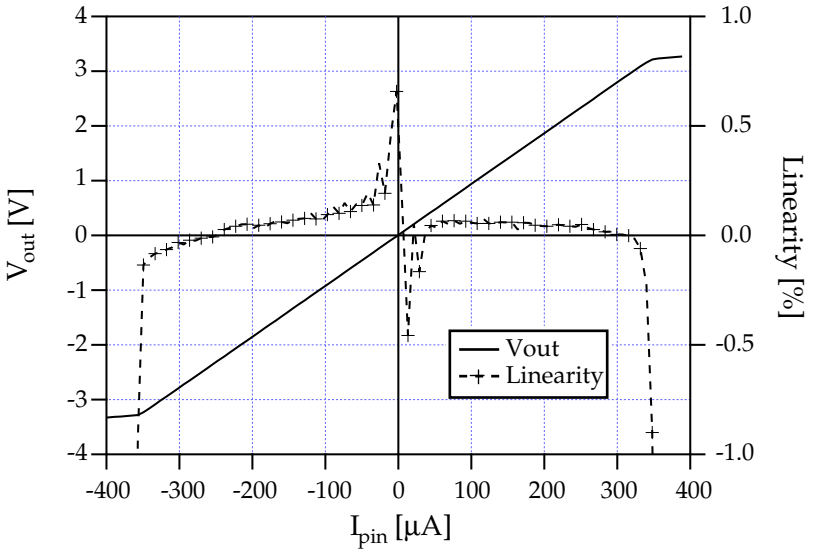


Fig. 9 : Photodiode amplifier static characteristic. The linearity is plotted against the right axis.

*Dynamic characteristic*

The amplifier step response and settling time is shown in Fig. 10. Plotted is the 100 µA amplitude input step signal, the output signal after correction for any time delay, and their relative deviation in percent on the right axis. Both input and output signals were normalized to their stable value at 90 ns The noise on the relative deviation curve is the digitization noise of the 8 bits resolution oscilloscope. The spike at 70 ns corresponds to the coax cable reflection. A settling time of ≤12 ns to within 1% of the end value is achieved.

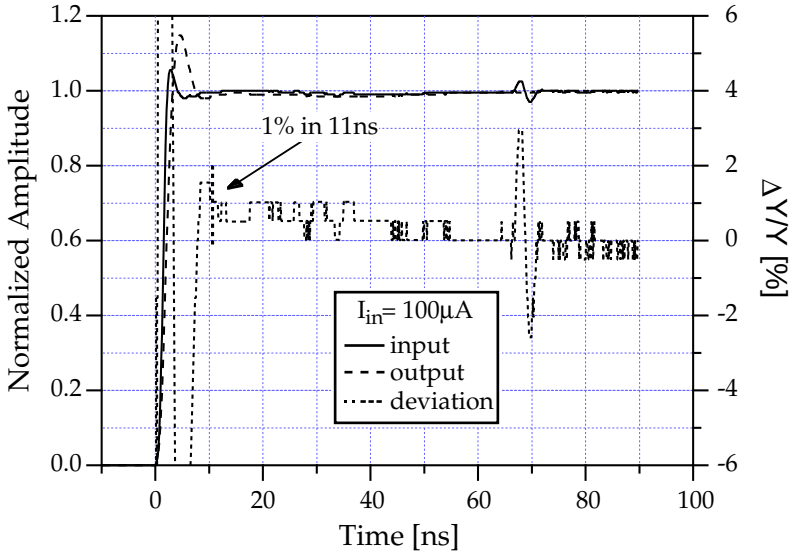


Fig. 10 : Receiver settling time to a step input signal.

The dynamic characteristic of the complete receiver module will essentially be limited by the amplifier bandwidth since the photodiode capacitance is only ≈ 1.5 pF at 5V reverse bias.

The overall time delay of the present amplifier is ≈ 3.3 ns and it was measured in the same way as for the transmitter time delay.

# 4 Full link characteristic

For easy evaluation of the link in a laboratory environment, a modular test platform was realized. It consists of a mother board onto which independent transmitter and receiver daughter boards are plugged in. The flexible design allows to use these evaluation platforms to test analogue as well as digital links for control and timing signal distribution.

## 4.1 Static characteristic

The link gain is expressed as follows:

$$\frac{V_{out}}{V_{in}} = R_{Rx} \times R_{pin} \times \eta \times G_m \times IL_{connector} \qquad (2)$$

where $R_{Rx}$ is the receiver transresistance gain, $R_{pin}$ the photodiode responsivity, $\eta$ the laser slope efficiency, $G_m$ the laser driver transconductance, and $IL_{connector}$ the connector insertion losses. The transmitter and receiver fibre pigtails were linked using a FC-PC optical connector with an average insertion loss, $IL_{connector}$, of ≈ 0.2 dB. The static response of the full link measured at room temperature is shown in Fig. 11 (a).

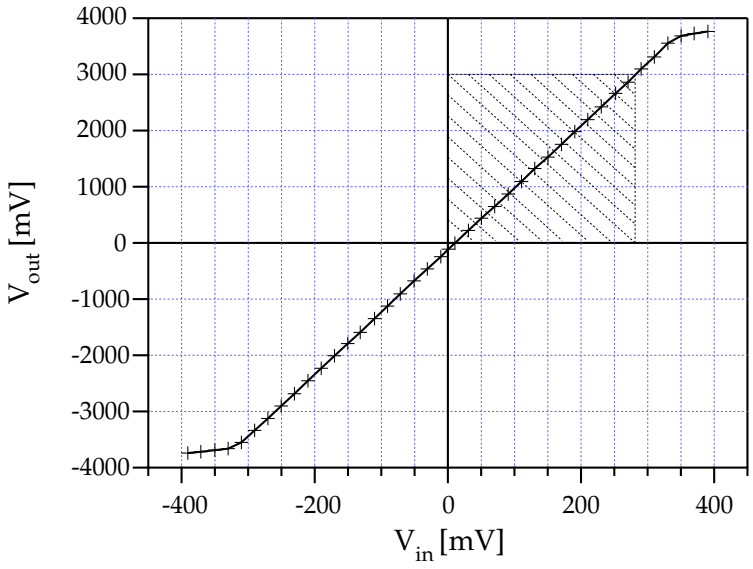


(a)

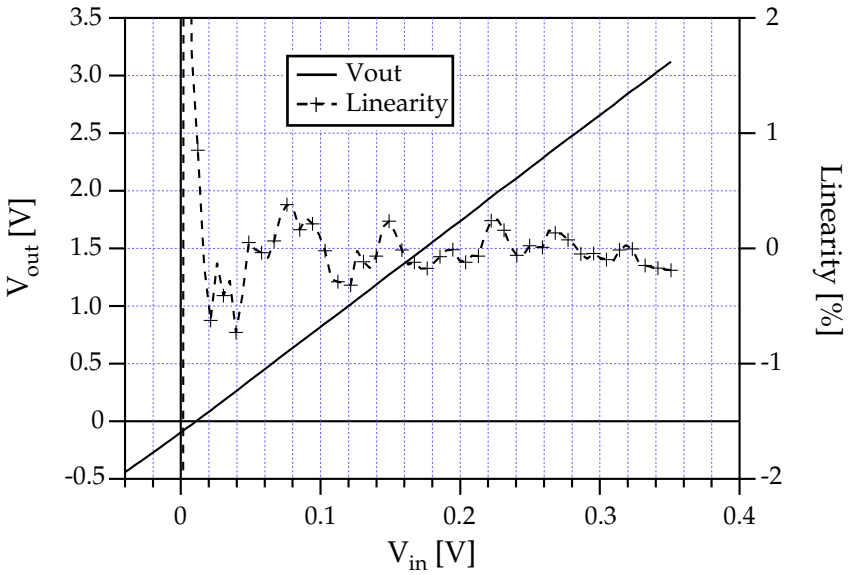


(b)

Fig. 11 : (a) Full link transfer characteristic. (b) Linearity over the 0-3V operating range of the ADC.

The laser and PIN diode were not temperature controlled. The hatched pattern represents the operating quadrant for ADC signals ranging between 0 and 3V, corresponding to injected signal levels between 0 and 300 mV. The experimental average link gain is 10.5, in close agreement with the 10.3 gain value computed from the independent link component characteristics using Eq. 2. It is worth noting that uncertainty arises from $IL_{connector}$ since the insertion losses depend on the mating and/or remating reproducibility.

The relative deviation from linearity (RDL) for the top right quadrant is shown in Fig. 11 (b) where the input voltage was increased in steps of ≈ 3.5 mV. It is calculated from the relative error with respect to a linear fit for input signals between 0 and 300 mV, in the same way as was previously done for the laser driver and photodiode amplifier (see Eq. 1). The full link relative distortion with the current optoelectronic components is well within the 2% linearity specification.

### 4.2 Dynamic characteristic

The link demonstrator step response is shown in Fig. 12. The straight line is the input signal with the scale on the left axis. The dashed line represents the output signal and is plotted against the right axis. The input pulse is typical of a large signal delivered by the front-end APV chip with a rise time of 5ns and a plateau of 20ns. We measure on the output pulse an overshoot of ≈ 20% of the pulse height and a settling time of 15ns to within 1% of

the end value. It is worth recalling that signals will have to be digitized within the 25ns of the sample period.

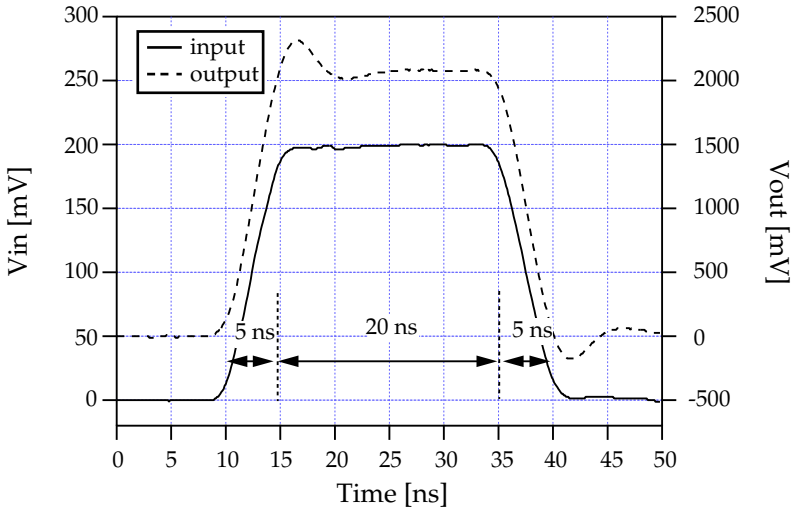


Fig. 12 : Full link step response to an APV representative signal.

The full link frequency response characteristic, shown in Fig. 13, was measured using a spectrum analyzer equipped with a tracking generator. The stimulus input signal was sinusoidal with amplitude V(rms) ≈ 75 mV and frequencies between 1MHz and 250 MHz. The experimental points (dots on Fig. 13) are compared to a line fit based on a second order filter analytical model.

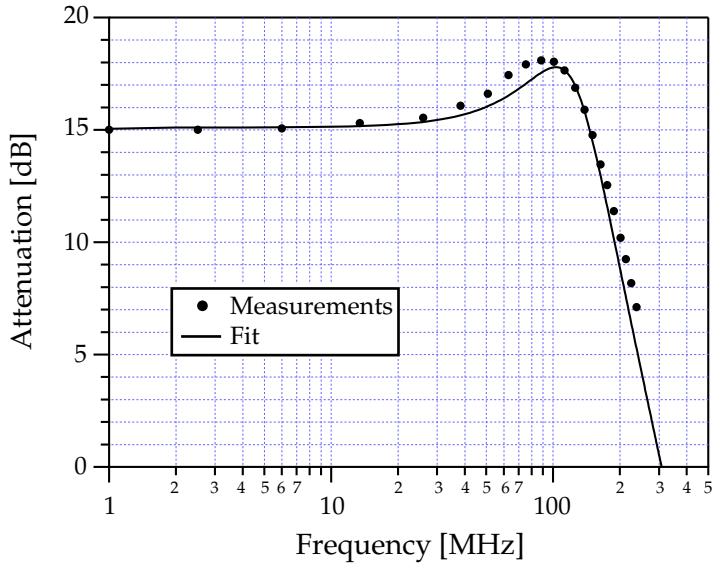


Fig. 13 : Full link frequency response. Dots are the experimental data and the line is a fit using a second order filter.

The static link gain is 15.1 dB (into 50Ω) and is consistent with the dc gain value mentioned above (into high impedance). The -3dB cut-off frequency is 180 MHz, essentially limited by the receiver bandwidth. Also, a +3dB resonance peak is observed at around 90 MHz causing the ringing behaviour visible in the time domain (Fig. 12). By applying an inverse Fourier transformation on the fit, the temporal step response was synthesized and the measured 15ns settling time value within 1% was confirmed (see Fig. 14).

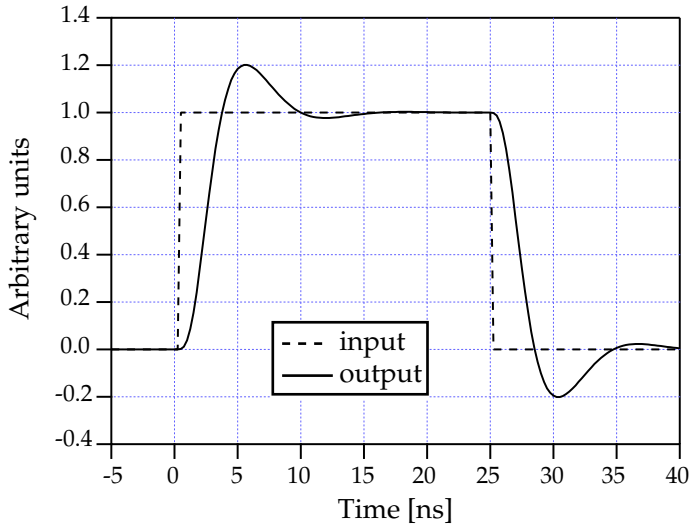


Fig. 14 : Temporal step response calculated from the inverse Fourier transformation of the link frequency spectrum (approximated as a 2nd order minimal phase network).

In order to improve the damping and better compensate the system response, a first order RC filter was added to the second stage of the receiver (a peaking capacitor in parallel with the feedback resistor). The optimization of this first order filter cut-off frequency was realized with the help of an analytical model [19]. The resulting frequency and temporal responses for a filter bandwidth close to 70 MHz are shown in Fig. 15(a) and 15(b). Data without this extra filter (as in Fig. 12 and Fig. 13) are also plotted for comparison. The new link bandwidth is equal to 110 MHz, corresponding to a bandwidth reduction of a factor of ≈ 1.6 (180 MHz/110 MHz), and the overshoot in the time domain is now limited to only a few percent of the pulse height. This bandwidth reduction should theoretically augment the SNR by ≈ √1.6, as will be demonstrated in the next section. In addition, the settling time did not degrade with this additional damping filter, in perfect agreement with the model.

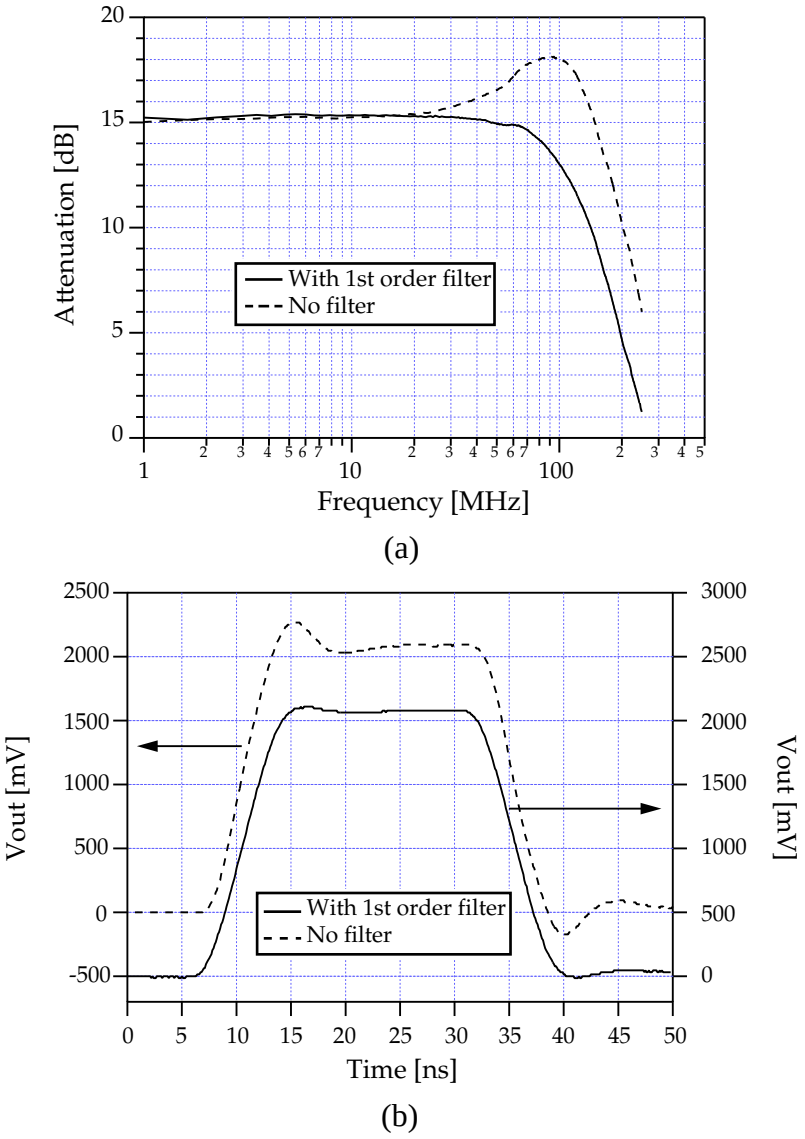


Fig. 15 : Effect of a first order filter on the (a) frequency and (b) temporal responses of the full link. The input signal of the step response is the one shown in Fig. 12 with an amplitude of 200 mV.

### 4.3 Noise

The link noise was measured with and without the compensating filter. Results are reported in Fig. 16 with the equivalent input noise spectral density and integrated rms noise on the left and right axis, respectively. The equivalent input rms noise (in the full link frequency bandwidth) is ≈ 1.5 mV for the bare link and ≈ 1.1 mV for the compensated link. As already mentioned, this noise reduction is in close agreement with the theoretically predicted square root of the bandwidth ratio ( $(BW_{no\text{-}filter}/BW_{filter})^{1/2}$) improvement factor. The corresponding peak signal to rms noise ratio is ≥ 250/1 (assuming a 300 mV input peak signal).

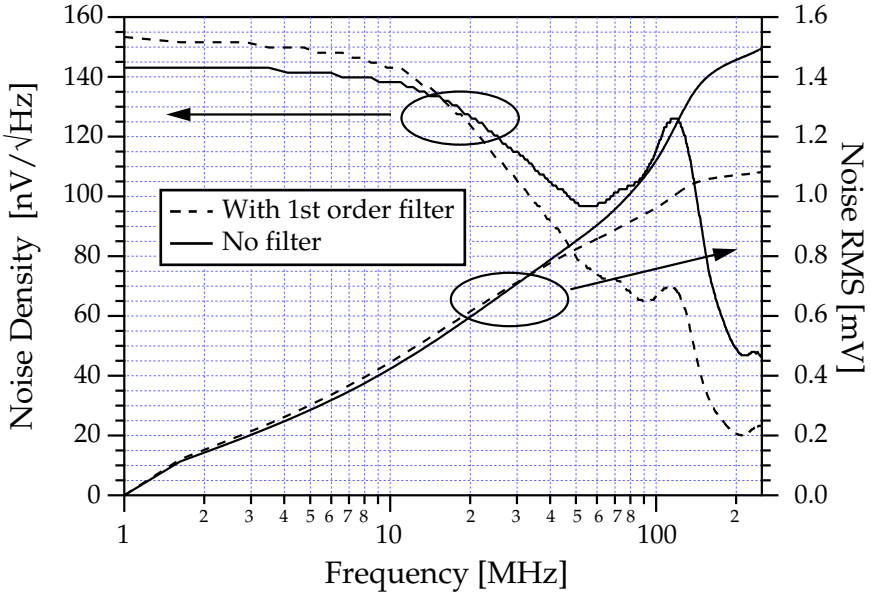


Fig. 16 : Full link equivalent input noise spectral density and rms noise.

It was discovered late in the link characterization procedure that the link noise obtained with the laser used during our experiment was significantly higher than the average noise measured within our laser batch. As illustrated in Fig. 17, a more representative laser gives a low equivalent input rms noise value of ≈ 0.7 mV corresponding to a peak SNR ≈ 420/1.

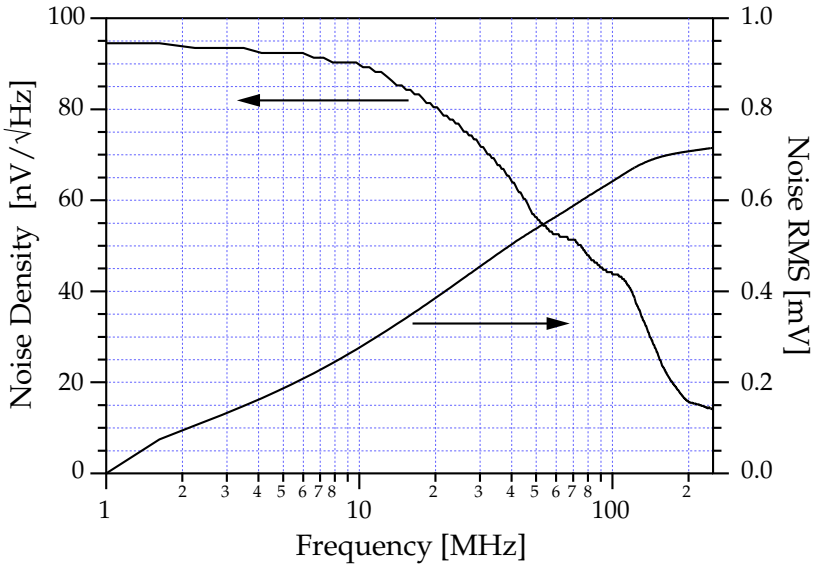


Fig. 17 : Equivalent input noise figure of the full link with laser representative of our laser population.

It can be seen in Figs. 16 and 17 that the noise spectral density is not flat over the link bandwidth, with a small decline already starting at ≈ 10 MHz. The link noise is thus not of the white type. The different noise budget items are the thermal or Johnson noise of the electronics, the relative intensity noise (laser RIN) or phase fluctuations inherent to the lasing action [20], and the phase to intensity noise generated by interferometric cavities from interfaces along the link. Work is in progress to determine and locate the major noise sources of our optical link.

## 5 Conclusion

A prototype link demonstrator based on commercially available optoelectronic devices has been built and fully characterized. Directly modulated 1310 nm semiconductor lasers (to be located inside the detector volume) are driven by transconductance amplifiers. The laser light is transmitted by single-mode optical fibres to the receiver circuit boards where it is detected by reverse biased PIN photodiodes coupled to transimpedance amplifiers. The prototype driver and receiver amplifiers are built using commercial IC's. The lasers and PIN assemblies and packages are identical to the ones tested for radiation hardness. The development of 4-way links with laser driver ASIC's in rad-hard technology is under way.

The link characterization has been performed on highly modular evaluation platforms with independent transmitter and receiver circuit boards. The reported static and dynamic performances meet all the requirements for the electronic readout of the tracker with deviation from linearity < 1% and settling time <15ns to within 1% of the end value. The input equivalent rms noise using currently available lasers is of the order of ≈ 0.7 mV. With a full link cut-off frequency at 110 MHz, a SNR ≈ 420/1 has been demonstrated.

Links with evaluation platforms are now being made available to the CMS community.

## Acknowledgements

The authors would like to acknowledge Paolo Moreira for fruitful discussions. We also would like to thank Bernard Cornet for assistance in preparing the transmitter and receiver boards

## References


[1] G. Hall and G. Stefanini, “CMS tracker readout system”, CMS TN/94-137

[2] F. Vasey, G. Stefanini, and G. Hall, “Laser based optical links for the CMS tracker: options and choises”, CMS note 1997/053

[3] G. Hall, G. Stefanini, F. Vasey, “Fibre optic link technology for the CMS tracker”, CMS note 1996/012

[4] RD23 status reports, CERN/DRDC 93-35 (1993), CERN/DRDC 94-38 (1994), CERN/DRDC 95-61 (1995), CERN/LHCC 97-30 (1997)

[5] MDM de Fez-Laso et al., “Beam test performance of the APV5 chip”, Nucl. Inst. and Meth. A382, 533 (1996)

[6] G. Hall, “Analogue optical data transfer for the CMS tracker”, Nucl. Inst. and Meth. A386, 138 (1997)

[7] The Compact Muon Solenoid Technical Proposal. CERN Report LHCC 94-38 (1994)

[8] M. Huhtinen, “Radiation environment simulations for the CMS detector”, CMS TN/95-198

[9] M. Huhtinen, “Studies of neutron moderator configurations around the CMS inner tracker and ECAL”, CMS TN/96-057

[10] K. Gill et al., “Effect of neutron irradiation of MQW lasers to $10^{15}$n/cm$^2$”, CMS Note 044 (1997)

[11] K. Gill et al., “Radiation damage studies of optoelectronic components for the CMS tracker optical links”, submitted for a CMS Note (1997)

[12] K. Gill et al., “Gamma and neutron radiation damage studies of optical fibres”, to be published in J. Non-Cryst. Solids (1997)

[13] G. Stefanini, “An overview of requirements for optical links in LHC experiments”, Proceedings of the first workshop on electronics for LHC experiments, Lisbon, 157 (1995)

[14] V. Arbet-Engels et al., “Analogue optical links for the CMS tracker readout system”, to be published in the Proceedings of the 7th Pisa Meeting on Advanced Detectors, special issue of Nucl. Inst. and Meth. A. (1997)

[15] G. P. Agrawal and N. K. Dutta, Semiconductor Lasers (Van Nostrand Reinhold, New York, 1993)

[16] A. M. Joshi, G. H. Olsen, and S. R. Patil, “Reliability of InGaAs detectors and arrays” SPIE vol. 1580, 34 (1991)

[17] G. P. Agrawal, Fiber-Optic Communication Systems (John Wiley & Sons, Inc., 1992)

[18] J. G. Graeme, Photodiode Amplifiers: Op Amp Solutions (McGraw-Hill, 1996)

[19] G. Cervelli, private communication

[20] K. Petermann, Laser Diode Modulation and Noise, (KTK Scientific Publishers/Tokyo - Kuwer Academic Publishers, 1991)